

Role of Nonlinear Coupling and Density Fluctuations in Magnetic-Fluctuation-Induced Particle Transport

L. Lin, W. X. Ding, D. L. Brower, W. F. Bergerson, T. A. Carter, and T. F. Yates

Department of Physics and Astronomy, University of California Los Angeles, Los Angeles, California 90095, USA

A. F. Almagri, B. E. Chapman, and J. S. Sarff

Department of Physics, University of Wisconsin–Madison, Madison, Wisconsin 53706, USA

(Received 4 October 2011; published 23 April 2012)

Three-wave nonlinear coupling among spatial Fourier modes of density and magnetic fluctuations is directly measured in a magnetically confined toroidal plasma. Density fluctuations are observed to gain (lose) energy from (to) either equilibrium or fluctuating fields depending on the mode number. Experiments indicate that nonlinear interactions alter the phase relation between density and magnetic fluctuations, leading to strong particle transport.

DOI: [10.1103/PhysRevLett.108.175001](https://doi.org/10.1103/PhysRevLett.108.175001)

PACS numbers: 52.25.Gj

Magnetic-fluctuation-induced particle transport is an increasingly important topic in astrophysics [1] and high-temperature laboratory plasma research [2]. For magnetically confined fusion plasmas, magnetic fluctuations arising from microtearing modes [3], global tearing modes [4], and energetic-particle-induced instabilities [5], as well as from external-coil-induced resonant-magnetic perturbations used to mitigate edge-localized modes [6], can all act to enhance particle transport. In addition, magnetic fluctuations leading to a stochastic magnetic field have also been observed in recent gyrokinetic simulations of the drift-wave type of turbulence, after inclusion of finite pressure effects [7]. The effect of magnetic fluctuations on particle transport is predicted to increase with β (ratio of plasma pressure to magnetic field pressure) and to be important for burning plasmas where 3.5 MeV α particles are available to drive instabilities [8]. Understanding the physics of particle transport associated with magnetic fluctuations is critical for maintaining plasma confinement, density control, and impurity exhaust in burning plasmas like those in ITER and beyond.

Direct measurements of magnetic-fluctuation-induced transport in high-temperature plasmas are rare [4], being largely limited by methods available to access the hot plasma core. Recent measurements [9] have established that magnetic-fluctuation-induced particle transport, arising from the correlated product of density and magnetic fluctuations, is the cause of the density profile relaxation during quasiperiodic relaxation events (or sawtooth crashes) in the reversed-field pinch (RFP). Despite different magnetic topologies, sawtooth crashes in RFPs and tokamaks have many common features, including density and current profile relaxation as well as increased turbulence [10,11]. During the crash, the RFP magnetic field is strongly stochastic and the phase between density and magnetic fluctuations is observed to change so as to induce transport. In addition, the observed particle transport [9] is

much larger than expected from the quasilinear prediction [12] for ambipolar particle transport in a stochastic field, suggesting that coherent, nonlinear, mode-mode interactions might serve to drive this transport.

Nonlinear interactions between density and electrostatic potential fluctuations associated with drift-wave turbulence have been extensively studied previously ([13,14], and references therein). In this Letter, we report on direct measurements of a broad spectrum of nonlinear three-wave interactions between density and magnetic fluctuations associated with global tearing instabilities. Energy exchange between different spatial Fourier modes resulting from nonlinear interactions acts to drive or damp density fluctuations, depending on the mode number. These measurements reveal that the effects of nonlinear three-wave interactions are comparable to linear advection where energy exchange with the equilibrium density gradient occurs. Nonlinear interactions are observed to alter the phase relation between density and magnetic fluctuations so as to drive large particle transport.

Following a similar approach as in Ref. [15] and starting from the continuity equation for incompressible electrons ($\nabla \cdot \mathbf{v}_e \approx 0$), we can write

$$\frac{\partial n_e}{\partial t} + \mathbf{v}_e \cdot \nabla n_e \approx S_e, \quad (1)$$

where n_e , \mathbf{v}_e , and S_e are the electron density, velocity, and source term, respectively. n_e and \mathbf{v}_e can be decomposed into their equilibrium (n_0 and \mathbf{v}_0) and fluctuating (\tilde{n}_k and $\tilde{\mathbf{v}}_k$) components, i.e., $n_e = n_0 + \sum_k \tilde{n}_k$ and $\mathbf{v}_e = \mathbf{v}_0 + \sum_k \tilde{\mathbf{v}}_k$, where $k = (m, n)$ and m and n are the poloidal and toroidal mode numbers, respectively. Here, we focus on the radial velocity fluctuations (\tilde{v}_r) associated with particles streaming along the fluctuating magnetic field. From the field line equation, we obtain $\tilde{v}_r = v_{e\parallel} \tilde{b}_r / B_0$, where $v_{e\parallel}$ denotes the parallel electron drift velocity along the field line, \tilde{b}_r is the radial magnetic fluctuation, and B_0 is the equilibrium

magnetic field. After substituting the decomposed n_e and \mathbf{v}_e into Eq. (1), multiplying by \tilde{n}_{k_1} , substituting for \tilde{v}_r , and performing an average $\langle \dots \rangle$ over the magnetic flux surface, we have the energy equation for electron density fluctuations:

$$\frac{1}{2} \frac{\partial \langle \tilde{n}_{k_1}^2 \rangle}{\partial t} \simeq - \frac{v_{e\parallel}}{B_0} \langle \tilde{n}_{k_1} \tilde{b}_{r,k_1} \rangle \frac{\partial n_0}{\partial r} - \frac{v_{e\parallel}}{B_0} \sum_{k_1=k_2 \pm k_3} \left\langle \tilde{n}_{k_1} \tilde{b}_{r,k_2} \frac{\partial \tilde{n}_{k_3}}{\partial r} \right\rangle. \quad (2)$$

Contributions from the source, higher-order nonlinear interactions (such as four-wave coupling), and dissipation effects are not considered. The left-hand side of Eq. (2) is the power term describing the temporal evolution of modal energy residing in \tilde{n}_{k_1} . The first term on the right-hand side represents linear advection, which accounts for the energy exchange between \tilde{n}_{k_1} and the equilibrium density gradient $\partial n_0 / \partial r$. This term can also be written as $-\Gamma_{k_1} \partial n_0 / \partial r$, where $\Gamma_{k_1} = v_{e\parallel} \langle \tilde{n}_{k_1} \tilde{b}_{r,k_1} \rangle / B_0$ is the particle flux resulting from fluctuations with k_1 . The second term on the right-hand side results from nonlinear advection. It is a triple product of three fluctuating quantities (\tilde{n}_{k_1} , \tilde{b}_{r,k_2} , and $\partial \tilde{n}_{k_3} / \partial r$) and describes the nonlinear three-wave interaction among fluctuations with mode numbers k_1 , k_2 , and k_3 . Depending on the sign, the linear and nonlinear advection terms can act to drive or damp density fluctuations. In the following, we report on direct measurements of each term in Eq. (2).

Our experiments have been conducted in the Madison Symmetric Torus [16], a toroidal device with major radius $R = 1.5$ m and minor radius $a = 0.52$ m. All data presented herein are for deuterium RFP plasmas with toroidal plasma current 400 kA and central line-averaged electron density $1 \times 10^{19} \text{ m}^{-3}$. Multiple magnetic tearing modes resonate in these plasmas. Modes with $m = 1$ and $n = 5-12$ resonate inside the reversal surface, $r/a < 0.8$. Beyond this surface, the toroidal magnetic field reverses direction. Modes with $m = 0$ and $n = 1-4$ resonate at the reversal surface, where the electron temperature is ~ 150 eV. The plasma exhibits a quasiperiodic “sawtooth” relaxation cycle evident in many quantities [17]. The cycle consists of a slow ramp (~ 4 ms) followed by a rapid relaxation or crash ($\sim 100 \mu\text{s}$) during which the tearing modes spike to their maximum amplitudes. The multiple magnetic islands associated with these modes overlap, leading to a stochastic magnetic field [18] accompanied by strong density relaxation and particle pump-out [9].

Although tearing modes have localized resonant surfaces, their associated density (\tilde{n}_k) and radial magnetic fluctuations ($\tilde{b}_{r,k}$) have a global extent. All \tilde{n}_k 's peak near the reversal surface where the equilibrium density gradient ($\partial n_0 / \partial r$) is large [19], while $\tilde{b}_{r,k}$ peaks near the corre-

sponding resonant surface [20]. Measurements shown herein were obtained near the reversal surface where $m = 0$ modes are maximum. To illustrate typical behavior, the root-mean-square (rms) values of \tilde{n} , \tilde{b}_r , their relative phase $\delta_{\tilde{n}\tilde{b}_r}$, and the magnetic-fluctuation-induced particle flux $\Gamma_k = v_{e\parallel} \langle \tilde{n}_k \tilde{b}_{r,k} \rangle / B_0$, for the $(m, n) = (1, 10)$ mode, are shown in Fig. 1. The measurements are accomplished by using a high-speed, laser-based, polarimetry-interferometry diagnostic. The line-integrated measurements from the outermost chord are localized to the edge region ($0.8 \leq r/a \leq 1$). Standard interferometry is employed to measure the equilibrium density profile and density fluctuations. Electron drift velocity along the field line ($v_{e\parallel}$) is determined from $v_{e\parallel} = J_{\parallel} / (en_0)$, where J_{\parallel} is the parallel plasma current density and e is the electron charge. Radial magnetic fluctuations \tilde{b}_r , equilibrium magnetic strength B_0 , and J_{\parallel} are each determined by measuring the Faraday effect [20,21]. Detailed descriptions of the measurement and analysis techniques have been previously published [9,22]. For $t \leq -0.2$ ms, well before the sawtooth crash at $t = 0$ ms, although \tilde{n} [Fig. 1(a)] and \tilde{b}_r [Fig. 1(b)] have finite amplitude, their relative phase $\delta_{\tilde{n}\tilde{b}_r}$ [Fig. 1(c)] is close to $\pi/2$, resulting in a low particle flux [Fig. 1(d)]. However, at $t = -0.06$ ms, just before the crash, $\delta_{\tilde{n}\tilde{b}_r}$ deviates from $\pi/2$ as \tilde{n} and \tilde{b}_r amplitudes increase, leading to maximum particle flux at the crash. Similar observations have been made for the other $m = 1$ modes. This burst in flux causes density profile relaxation and particle pump-out [9].

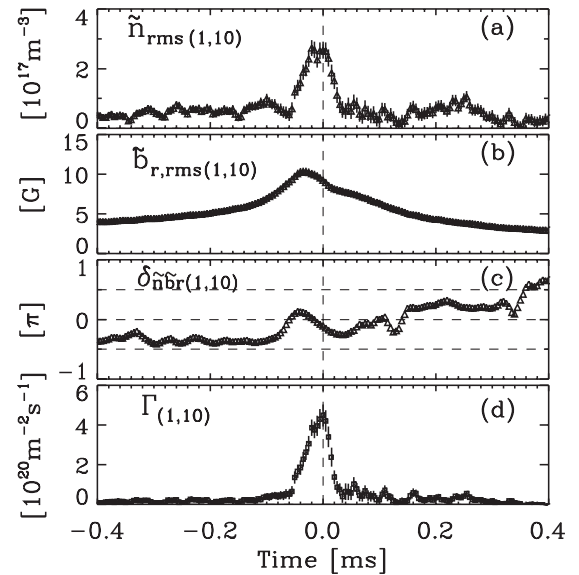


FIG. 1. Temporal evolution of the (a) rms value of density fluctuation (\tilde{n}), (b) rms value of radial magnetic fluctuation (\tilde{b}_r), (c) phase between \tilde{n} and \tilde{b}_r , and (d) magnetic-fluctuation-induced particle flux from the $(m, n) = (1, 10)$ mode at $r/a \sim 0.8$ during the sawtooth cycle. Crash occurs at $t = 0$.

Addressing the intriguing question of why the fluctuation amplitudes and phase spontaneously change at the crash requires investigation of driving and damping mechanisms of the density fluctuations through measurement of all terms in Eq. (2). To evaluate the linear and nonlinear terms, in addition to the results from Fig. 1, measurements of $\partial n_0/\partial r$ and $\partial \tilde{n}_k/\partial r$ are required. $\partial n_0/\partial r$ is obtained by taking the gradient of the inverted line-integrated density profile, while $\partial \tilde{n}_k/\partial r$ is directly measured by using a novel differential interferometry technique [22]. The amplitude of $\partial \tilde{n}_k/\partial r$ tracks that of \tilde{n}_k and peaks at the crash. After obtaining \tilde{n}_{k_1} , \tilde{b}_{r,k_2} , and $\partial \tilde{n}_{k_3}/\partial r$, their triple product can be quantitatively determined. The sign and amplitude determine the direction and strength of energy flow among the modes involved in the nonlinear interaction and are critical to understanding the underlying mechanisms of the three-wave process.

Evaluation of Eq. (2) for the $(m, n) = (1, 10)$ mode reveals that each of the three terms grows significantly at the sawtooth crash, as shown in Fig. 2. Interestingly, the measured power term is much smaller than the linear and nonlinear advection terms, remaining below $0.2 \times 10^{40} \text{ m}^{-6} \text{ s}^{-1}$. The magnitude of the linear and nonlinear terms begins to change at $t = -0.06$ ms before the crash, when \tilde{n} and \tilde{b}_r amplitudes increase, and their relative phase begins to deviate from $\pi/2$ [see Figs. 1(a)–1(c)]. The linear term is large and positive ($1.5 \times 10^{40} \text{ m}^{-6} \text{ s}^{-1}$ at $t = -0.02$ ms), which indicates that the $(1, 10)$ mode is linearly unstable as it gains its energy from the equilibrium density gradient $\partial n_0/\partial r$. In contrast, the nonlinear term is negative with comparable amplitude, indicating that the nonlinear interaction is a sink of energy which is transferred away from the $(1, 10)$ mode to other modes through three-wave interactions. Within experimental uncertainty, the sum of the nonlinear and linear advection terms equates with the power term, thereby balancing Eq. (2).

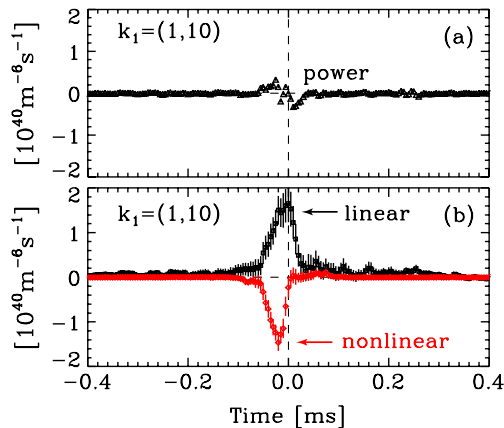


FIG. 2 (color online). Temporal evolution of the (a) power term and (b) linear (black line) and nonlinear (red line) advection terms for the $(m, n) = (1, 10)$ mode at $r/a \sim 0.8$ during a sawtooth cycle. Crash occurs at $t = 0$.

Similar analysis of Eq. (2) has been performed for all the dominant modes as shown in Fig. 3. Here we observe the mode spectra of linear and nonlinear terms averaged over the time interval -0.04 to -0.02 ms before the sawtooth crash. The power term is always small, remaining less than 15% of either the linear or nonlinear terms. The cause of the density fluctuations varies with the mode number as the linear and nonlinear advection terms can be either driving (positive) or damping (negative). Interestingly, the $m = 0$ and $n = 1, 2, 3, 4$ reversal-surface-resonant modes are all linearly stable and nonlinearly driven. The $m = 1$ core-resonant modes exhibit less uniform behavior. Modes ($m = 1$ and $n = 5-10$) with the longer wavelength and resonant surfaces closer to the magnetic axis are linearly unstable with nonlinear damping. Conversely, modes ($m = 1$ and $n = 11-12$) with the shorter wavelength and resonance closer to the reversal surface are nonlinearly driven with linear damping. In almost all cases, the linear and nonlinear terms are of opposite sign and roughly balance, within measurement error. There is an apparent energy imbalance for the $(0, 2)$ and $(0, 3)$ modes, as the amplitude of the nonlinear term is about half that of the linear term. This might be caused by three-wave interaction from $m \geq 2$ modes excluded in our analysis or other effects neglected in Eq. (2). Balancing linear and nonlinear advection leads to the relation

$$\Gamma_{k_1} \simeq -\frac{J_{\parallel}}{en_0 B_0} \left(\frac{\partial n_0}{\partial r}\right)^{-1} \sum_{k_1=k_2 \pm k_3} \left\langle \tilde{n}_{k_1} \tilde{b}_{r,k_2} \frac{\partial \tilde{n}_{k_3}}{\partial r} \right\rangle, \quad (3)$$

revealing that the magnetic-fluctuation-induced particle flux is affected by nonlinear interactions.

Many mode combinations can satisfy the sum rule ($k_1 = k_2 \pm k_3$) for the three-wave interactions, and the nonlinear terms shown in Figs. 2 and 3 are summed over all combinations. For example, the nonlinear interaction spectrum for the $(m, n) = (1, 10)$ mode is shown in Fig. 4, at $t = -0.02$ ms, when the nonlinear interaction is strongest. The nonlinear term is negative, and the energy is transferred

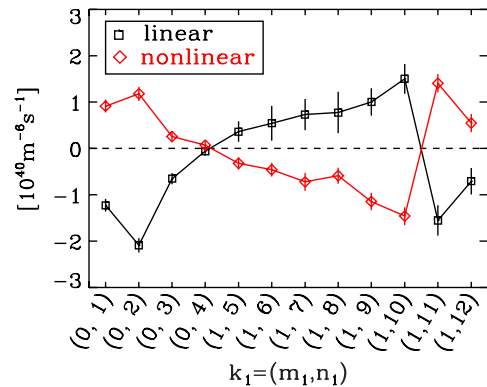


FIG. 3 (color online). Spectra of linear and nonlinear terms. Data are averaged over the interval $t = -0.04$ ms to $t = -0.02$ ms before the sawtooth crash.

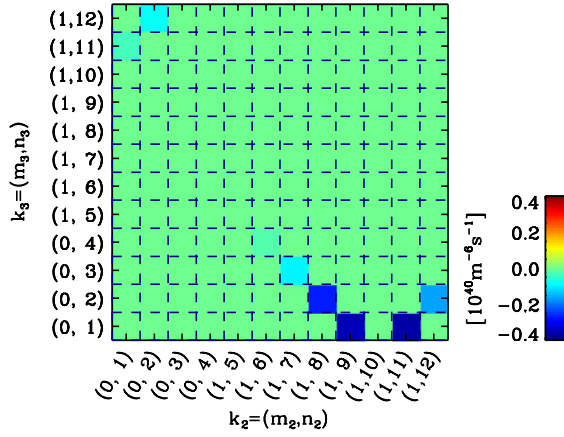


FIG. 4 (color online). Mode spectrum of nonlinear interaction for the $k_1 = (1, 10)$ mode at $t = -0.02$ ms and $r/a \sim 0.8$.

away from the $(1, 10)$ mode. The three-wave interactions with $(1, 9)$ and $(1, 11)$ modes have the largest amplitudes, indicating that the interaction is dominated by coupling with nearby or adjacent modes through the $(0, 1)$ mode. Smaller contributions come from the $(0, 2)$ and $(0, 3)$ modes. Similar observations have been made for the other $m = 1$ modes. To further explore the role played by the $(0, 1)$ mode, we have compared sawtooth cycles where the $(0, 1)$ mode peaks at the crash with those where the $(0, 1)$ mode exhibits no burst, as shown in Fig. 5(a). Both crash types occur spontaneously, although those with large $(0, 1)$ bursts are more typical. For these events, the core-resonant $m = 1$ modes also behave differently, as seen in Figs. 5(b) and 5(c), for the $(1, 7)$ mode. Measurements demonstrate

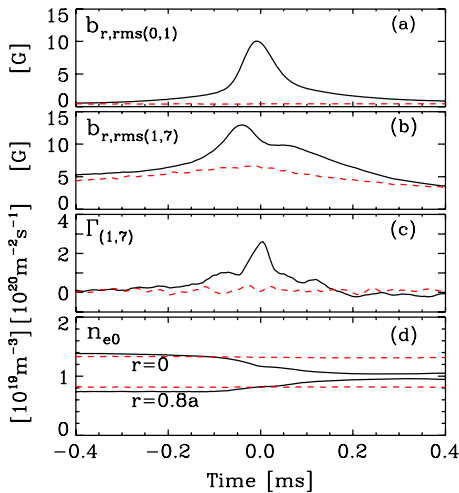


FIG. 5 (color online). For two types of sawtooth cycles: with a strong $(0, 1)$ burst (black solid line) and without a $(0, 1)$ burst (red dashed line), temporal evolution of the (a) $(0, 1)$ radial magnetic fluctuation, (b) $(1, 7)$ radial magnetic fluctuation, (c) $(1, 7)$ mode magnetic-fluctuation-induced particle flux at $r/a \sim 0.8$, and (d) equilibrium electron density at the core ($r \sim 0$) and reversal surface ($r/a \sim 0.8$).

that the magnetic-fluctuation increase is less pronounced and no significant particle flux is induced for the sawtooth crash where the $(0, 1)$ mode burst is not evident. Furthermore, comparison of the equilibrium density evolution [see Fig. 5(d)] reveals that density relaxation (decrease of the central density at $r \sim 0$ and increase of the edge density at $r/a \sim 0.8$) is no longer observed when the $(0, 1)$ mode amplitude is unchanged at the crash. For sawtooth crashes where the $(0, 1)$ mode is not evident, there is no burst in particle flux and no change in equilibrium density. Combining this observation with the nonlinear spectra in Fig. 4 confirms the importance of the $(0, 1)$ mode in mediating nonlinear three-wave interactions.

The nonlinear interaction is important in two aspects. First, it is responsible for phase deviation from $\pi/2$ and increased particle transport, confirming Eq. (3). If only linear advection exists, the phase between density and radial magnetic fluctuations remains near $\pi/2$ and only weak particle transport is induced. Second, the nonlinear interaction provides the balance for the linear advection in Eq. (2).

While the measurements presented herein were made in the environment of a stochastic magnetic field created by nonlinearly interacting tearing modes, Eq. (2) applies whether or not the field is stochastic. The particle transport described in this Letter is intrinsically associated with the coherent interaction of magnetic and density perturbations, implying that magnetic-fluctuation-induced particle transport could arise even in the absence of magnetic stochasticity. This may explain why electron transport during the sawtooth crash can exceed the ambipolar-constrained value expected for parallel streaming in a stochastic magnetic field [9].

In conclusion, direct experimental measurements of linear advection and nonlinear three-wave interactions have been made, revealing their effect on density fluctuations and magnetic-fluctuation-induced particle transport. Strong nonlinear coupling among global magnetic perturbations is approximately balanced by linear advection during reconnection and leads to enhanced particle transport.

The authors thank the Madison Symmetric Torus group for their support and contributions to this research. This work is supported by the U.S. Department of Energy.

- [1] E. P. Kontar, I. G. Hannah, and N. H. Bian, *Astrophys. J. Lett.* **730**, L22 (2011).
- [2] B. A. Carreras, *IEEE Trans. Plasma Sci.* **25**, 1281 (1997).
- [3] W. Guttenfelder, J. Candy, S. M. Kaye, W. M. Nevins, E. Wang, R. E. Bell, G. W. Hammett, B. P. LeBlanc, D. R. Mikkelsen, and H. Yuh, *Phys. Rev. Lett.* **106**, 155004 (2011).
- [4] M. R. Stoneking, S. A. Hokin, S. C. Prager, G. Fiksel, H. Ji, and D. J. Den Hartog, *Phys. Rev. Lett.* **73**, 549 (1994).
- [5] W. Heidbrink, *Phys. Plasmas* **15**, 055501 (2008).
- [6] T. E. Evans *et al.*, *Phys. Rev. Lett.* **92**, 235003 (2004).

- [7] W. M. Nevins, E. Wang, and J. Candy, *Phys. Rev. Lett.* **106**, 065003 (2011).
- [8] W. W. Heidbrink and G. J. Sadler, *Nucl. Fusion* **34**, 535 (1994).
- [9] W. X. Ding, D. L. Brower, G. Fiksel, D. J. Den Hartog, S. C. Prager, and J. S. Sarff, *Phys. Rev. Lett.* **103**, 025001 (2009).
- [10] D. L. Brower *et al.*, *Phys. Rev. Lett.* **65**, 337 (1990).
- [11] B. W. Rice and E. B. Hooper, *Nucl. Fusion* **34**, 1 (1994).
- [12] R. W. Harvey, M. G. McCoy, J. Y. Hsu, and A. A. Mirin, *Phys. Rev. Lett.* **47**, 102 (1981).
- [13] G. R. Tynan, A. Fujisawa, and G. McKee, *Plasma Phys. Controlled Fusion* **51**, 113001 (2009).
- [14] A. Fujisawa, *Plasma Phys. Controlled Fusion* **53**, 124015 (2011).
- [15] C. Holland, G. R. Tynan, R. J. Fonck, G. R. McKee, J. Candy, and R. E. Waltz, *Phys. Plasmas* **14**, 056112 (2007).
- [16] R. N. Dexter, D. W. Kerst, T. W. Lovell, S. C. Prager, and J. C. Sprott, *Fusion Technol.* **19**, 131 (1991).
- [17] S. Choi, D. Craig, F. Ebrahimi, and S. C. Prager, *Phys. Rev. Lett.* **96**, 145004 (2006).
- [18] T. M. Biewer *et al.*, *Phys. Rev. Lett.* **91**, 045004 (2003).
- [19] N. E. Lanier, D. Craig, J. K. Anderson, T. M. Biewer, B. E. Chapman, D. J. Den Hartog, C. B. Forest, S. C. Prager, D. L. Brower, and Y. Jiang, *Phys. Plasmas* **8**, 3402 (2001).
- [20] W. X. Ding, D. L. Brower, D. Craig, B. H. Deng, G. Fiksel, V. Mirnov, S. C. Prager, J. S. Sarff, and V. Svidzinski, *Phys. Rev. Lett.* **93**, 045002 (2004).
- [21] D. L. Brower, W. X. Ding, S. D. Terry, J. K. Anderson, T. M. Biewer, B. E. Chapman, D. Craig, C. B. Forest, S. C. Prager, and J. S. Sarff, *Phys. Rev. Lett.* **88**, 185005 (2002).
- [22] L. Lin, W. X. Ding, D. L. Brower, W. F. Bergerson, and T. F. Yates, *Rev. Sci. Instrum.* **81**, 10D509 (2010).